Resonant Bend Loss in Leakage Channel Fibers

R. A. Barankov[1,*], K. Wei[2], B. Samson[2], S. Ramachandran[1,*]

[1] *Photonics Center, Department of Electrical and Computer Engineering, Boston University, 8 Saint Mary's Street, Boston, Massachusetts 02215, USA*

[2] *Nufern, East Granby, Connecticut 06026, USA*

[*] *Corresponding authors: barankov@bu.edu, sidr@bu.edu*

Compiled May 22, 2012

Leakage channel fibers, designed to suppress higher-order modes, demonstrate resonant power loss at certain critical radii of curvature. Outside the resonance, the power recovers to the levels offset by the usual mechanism of bend-induced loss. Using C^2-imaging, we experimentally characterize this anomaly and identify the corresponding physical mechanism as the radiative decay of the fundamental mode mediated by the resonant coupling to a cladding mode.

OCIS codes: 060.2300, 060.2400, 060.3510

Resonantly enhanced leakage-channel fibers (LCFs) with large mode areas are designed to provide high-power propagation of diffraction-limited beams in high-power fiber lasers [1]. The microstructure of these fibers is tailored to enhance the loss of higher-order modes (HOMs) while maintaining tolerable loss of the fundamental mode, resulting in single-mode operation with large field diameters. In the existing designs [1], the index-continuity at the boundary in the azimuthal direction is broken. As a result, all modes propagating in the fiber are coupled to the radiative modes. However, the presence of gaps at the interface naturally promotes significant differential power-loss dominated by HOMs [1].

The physical mechanism underlying the LCF design suggests sensitivity of light propagation to the coiling conditions of the fibers. Coiled LCFs experience additional power loss resulting from the usual bend-induced coupling of the guided modes to the radiative modes [2–5]. This mechanism is illustrated in Fig. 1(e), where the core modes propagating in the slanted index-profile, representing the effect of fiber-bending, directly couple to the radiative modes. Certainly, the loss is significantly higher for HOMs than for the fundamental mode, as dictated by a narrower tunneling barrier.

This bend-loss becomes significant for small enough coiling radii [6]. The critical radius has been estimated, in the case of photonic-crystal fibers [7], as $R_c \sim \Lambda^3/\lambda^2$ in the short-wavelength limit, where λ is the wavelength of light, and Λ is the characteristic core size [7, 8]. This estimate should also hold for leakage-channel fibers characterized by similar geometry. For example, for the LCFs with core size $\Lambda \sim 50\,\mu$m, significant bend loss is expected at $R_c \sim 10\,$cm in the $1\,\mu$m spectral range.

In addition, bending of fibers induces intermodal coupling of the modes. The coupling increases dramatically when the effective indices of the two modes approach one another as a function of the fiber curvature as shown in Fig. 1(e). The anti-crossing occurs at some critical radius, which, in general, depends on the properties of

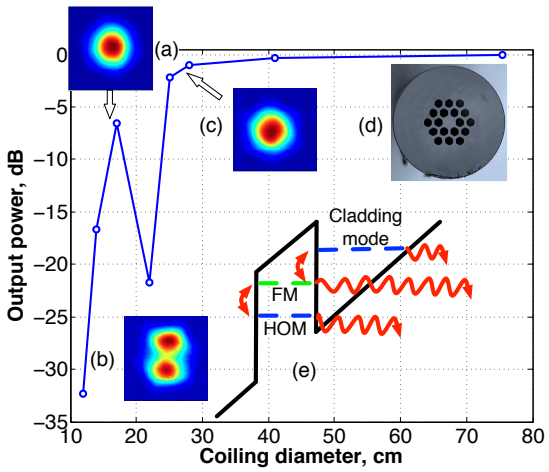

Fig. 1. (color online) Output power as a function of coiling diameter. *Insets* (a-c): Output mode profiles at different coiling diameters; (d) Cross-section of the LCF; (e) Power loss mechanisms in bent fibers

the coupled modes [9, 10]. Specifically, the fundamental mode can couple to a leaky HOM of the core, or to a quasi-guided cladding mode, as described in [11, 12], which leads to strong attenuation of light power.

In this work, we explore the interplay of these effects in a large-mode area LCF and observe an enhanced power loss at a certain coiling diameter. The results of power measurements in the 1-μm spectral range are shown in Fig. 1. Specifically, we find that for non-critical coiling radii, light propagation is dominated by the fundamental mode, as output near-field images in Fig. 1(a) and (c) illustrate. Thus, at non-critical radii the power-loss can be explained by the usual bend-loss mechanisms [2, 7]. In contrast, at the critical coiling radius, a higher-order mode dominates light propagation as shown in Fig. 1(b). While simple bend-loss measurements in Fig. 1 reveal this anomalous behavior, they do not identify the phys-

ical mechanism. We characterize the observed anomaly by the C^2-imaging method [13] and find that the effect is dominated by the resonant mode coupling of the fundamental mode to a quasi-guided cladding mode [11,12]. As a result, this method provides critical feedback for future fiber-designs, in which the critical radius R_c should be defined for specific amplifier packaging constraints.

The tested LCF of 285-cm-length has a core diameter of 50 μm and cladding diameter of 400 μm. The two rings of low-index (fluorine-doped) silica regions shown in Fig. 2(a) provide the leakage channel. The core, made of silica, is index matched to the outer silica glass. A high-index regular acrylate coating applied to the cladding ensures stripping of the cladding modes. The LCF has been designed to have negligible HOM content at lengths greater than 3 m. The input end of the fiber was spliced to a single-mode fiber to provide the same in-coupling conditions throughout the experiments.

The modal content of the LCF was analyzed using the C^2-imaging method [13] modified to account for elliptical polarization of the test beam. The basic idea of the method is to study the interference of the test beam with an external reference beam, and detect different waveguide modes in time-domain by changing the relative optical paths of the two beams.

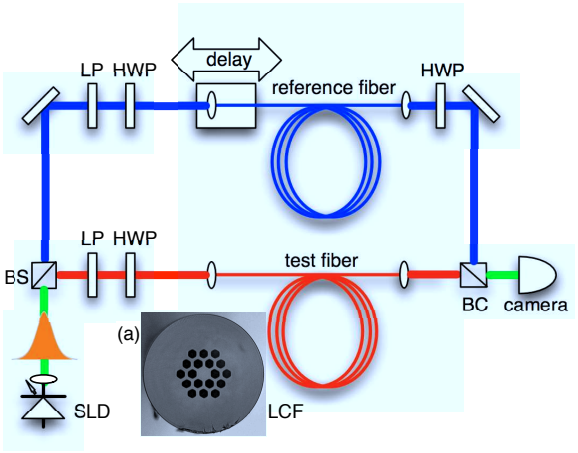

Fig. 2. (color online) C^2-imaging setup: SLD – superluminescent diode, LP – linear polarizer, HWP – half-wave plate, BS – beam-splitter, BC – beam combiner. *Inset* (a): Cross-section of the LCF

Figure 2 shows a schematic diagram of the experimental setup based on a Mach-Zehnder interferometer. We used a superluminescent diode (SLD) source centered at $\lambda \sim 1050$ nm with a spectral width of ~ 30 nm. The output beam of the LCF (focused at the imaging plane) interferes with the collimated reference beam radiated from the reference fiber. The length of polarization-maintaining reference fiber is chosen to compensate for the optical path difference between the two paths and also to reduce the effects of group-velocity dispersion of the LCF. The latter is important since we employ a light source with a relatively broad spectrum, which, in the absence of dispersion compensation, leads to significant dispersive broadening of the cross-correlation signal. In particular, the mode-specific resolution of the C^2-imaging method is defined by the spectral width of the source and also by the dispersion mismatch of the reference and test modes. In large-mode-area LCFs, the material dispersion dominates spectral broadening, which results in similar dispersion properties of HOMs. We chose the length of the reference fiber to match the material dispersion of LCF and, thus, reduced the dispersive broadening of all the modes simultaneously.

The cross-correlation signal $\mathcal{P}(\mathbf{r},\tau)$ as a function of the group delay τ and the coordinate $\mathbf{r}$ in the imaging plane is detected by the camera for different delay-stage positions $d = c\tau$ (c is the speed of light in vacuum):

$$\mathcal{P}(\mathbf{r},\tau) = \sum_m p_m \mathcal{G}^2_{mr}(\tau - \tau_{mr}) I_m(\mathbf{r}). \qquad (1)$$

Here, the summation extends over the modes propagating in LCF, p_m is the relative modal power of m-th mode ($\sum_m p_m = 1$), $\mathcal{G}_{mr}(\tau)$ is the mutual coherence function of the reference and test beams, $I_m(\mathbf{r})$ is the modal intensity, and τ_{mr} is the relative group delay of the m-th mode with respect to the reference mode.

Coiling of the fiber affects polarization properties of the test beam. To extract the power of every elliptically-polarized mode, we have recorded the cross-correlation trace for two orthogonal polarization states of the reference beam. The resulting trace, combining the two measurements, is represented in Eq. (1). The intensity distribution $I_m(\mathbf{r})$ of every mode was obtained by integrating this expression over the time extent of the mode. The relative power of the modes is encoded in the net cross-correlation trace obtained by integration of the spatially-dependent trace in Eq. (1) over the imaging plane position.

The result of this procedure, applied to the cross-correlation traces recorded at the critical coiling radius, is shown in Fig. 3. In this figure, the cross-correlation peaks identify the modes propagating in the fiber at the corresponding relative group delays. The shape of the peaks reflects the corresponding mutual coherence functions, while the peak values encode the relative power of the modes. The insets demonstrate the intensities of the reconstructed modes.

The dependence of the output power on the coiling diameter was measured using a power meter (as shown earlier in Fig. 1). Interestingly, we observe a dramatic decrease of the output light power at a specific coiling diameter $R_{exp} \approx 11$ cm, which is close to the estimate $R_c \sim 10$ cm for the onset of substantial power-loss. At this resonant coiling condition, the output image demonstrates domination of HOMs as shown in Fig. 1(b), while the output images in Fig. 1(a) and 1(c), recorded at coiling diameters outside the resonance, indicate single-mode operation. These measurements, however, do not indicate which of the two probable mechanisms, – the

intermodal coupling of the leaky core modes or the coupling between a core mode and quasi-guided cladding mode, – is responsible for the observed resonant behavior.

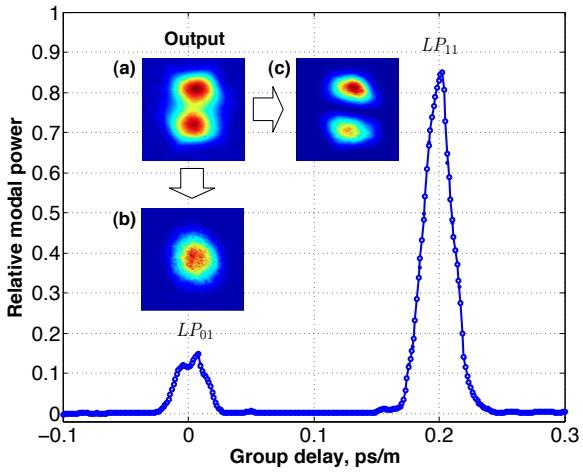

Fig. 3. (color online) Relative modal power as a function of group delay at the resonance ($R_c = 11$ cm). *Insets* (a-c): output image and the images of reconstructed modes

C^2-imaging [13] provides insight into the resonant behavior. The envelope of the integrated correlation trace shown in Fig. 3 at the critical coiling diameter demonstrates two modes (LP_{01} and LP_{11}) propagating with a relative group delay of about 0.2 ps/m, with the fundamental mode contributing only about 15% of the total power. In contrast, at other coiling diameters, HOMs are suppressed at power levels below −25 dB, as shown in Fig. 4. The well-defined group delay between the strongly attenuated fundamental mode and HOM suggests that the former resonantly couples to a cladding mode, as shown in Fig. 4(a). In the alternative mechanism, coupling between the core modes would lead to the appearance of a broad feature in C^2 trace due to the distributed nature of the coupling, and thus can not be detected by this method. However, the mechanism, if present, may affect the observed modal power distribution. In a set of similar measurements conducted on an LCF of smaller length of about 180 cm, a relatively shallow resonance was found at the same coiling diameter, with the relative group delay of ~ 0.2 ps/m between LP_{01} and LP_{11} modes. Likewise, we expect significantly deeper resonances for longer fiber lengths.

In summary, coiled few-mode fibers experience bend-induced coupling between the core and cladding modes as well as power-loss via direct coupling of core modes to the radiative modes. Using C^2-imaging, we explore the interplay between these phenomena in LCFs. We identify a resonant power-loss mechanism, in which a cladding mode mediates the coupling of the fundamental mode to the radiative modes. The effect becomes evident at a specific coiling diameter, where we observe a dramatic decrease of the output power. Outside the resonance, the power recovers to the levels determined by the usual bend-loss mechanism. We expect that quantitative characterization of this type would be critical in fiber laser applications using LCFs, since allowed coiling diameters would directly impact packaging conditions of high-power fiber-lasers.

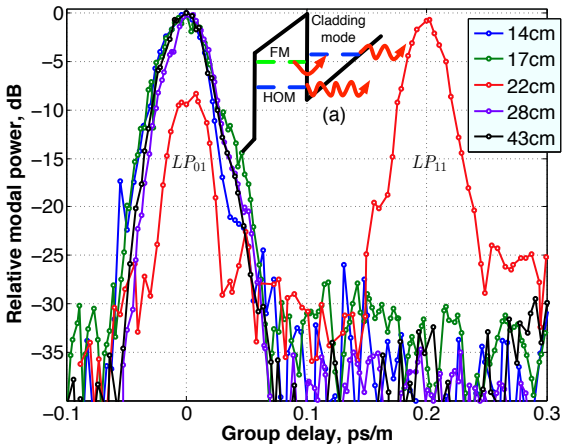

Fig. 4. (color online) Relative modal power of LP_{01} and LP_{11} (peak values) as a function of the relative group delay, for different coiling diameters. *Inset* (a): Bend-induced coupling of the FM and cladding mode as a mechanism of power-loss

This work was done with the support of ARL Grant No. W911NF-06-2-0040 and ONR grant nos. N00014-11-1-0133 & N00014-11-1-0098.

References

1. L. Dong, H. A. Mckay, A. Marcinkevicius, L. Fu, J. Li, B. K. Thomas, and M. E. Fermann, J. Lightwave Technol. **27**, 1565–1570 (2009).
2. D. Marcuse, J. Opt. Soc. Am. **66**, 216–220 (1976).
3. W. Wong, X. Peng, J. McLaughlin, and L. Dong, Opt. Lett. **30**, 2855–2857 (2005).
4. L. Dong, J. Li, and X. Peng, Opt. Express **14**, 11512–11519 (2006).
5. K. Saitoh, S. Varshney, K. Sasaki, L. Rosa, M. Pal, M. C. Paul, D. Ghosh, S. K. Bhadra, and M. Koshiba, J. Lightwave Technol. **29**, 2609–2615 (2011).
6. J. D. Love, Proc. Inst. Electr. Eng. Part J **13**, 225 (1989).
7. T. A. Birks, J. C. Knight, and P. S. Russell, Opt. Lett. **22**, 961–963 (1997).
8. M. D. Nielsen, N. A. Mortensen, M. Albertsen, J. R. Folkenberg, A. Bjarklev, and D. Bonacinni, Opt. Express, **12**, 1775–1779 (2004).
9. J. D. Love and C. Durniak, IEEE Ph. Techn. Lett. **19**, 1257–1259 (2007).
10. L. Yao, T. A. Birks, and J. C. Knight, Opt. Express, **17**, 2962–2967 (2009).
11. Y. Murakami and H. Tsuchiya, IEEE J. Quantum Electron., **QE-14**, 495–501 (1978).
12. H. Renner, J. Lightwave Technol. **10**, 544–551 (1992).
13. D. N. Schimpf, R. A. Barankov, and S. Ramachandran, Opt. Express **19**, 13008–13019 (2011).